Laser pulse ionization of fixed-in-space H_2O

2012 J. Phys. B: At. Mol. Opt. Phys. 45 194009

(http://iopscience.iop.org/0953-4075/45/19/194009)

J. Phys. B: At. Mol. Opt. Phys. **45** (2012) 194009 (7pp) doi:10.1088/0953-4075/45/19/194009

Laser pulse ionization of fixed-in-space H_2O

R Della Picca[1,4], J Fiol[1], P D Fainstein[1], J P Hansen[2] and A Dubois[3]

[1] CONICET and Centro Atómico Bariloche, Comisión Nacional de Energía Atómica, Avda E. Bustillo 9500, 8400 Bariloche, Argentina
[2] Department of Physics and Technology, University of Bergen, N-5007, Norway
[3] Laboratoire de Chimie Physique-Matière et Rayonnement, UPMC Université Paris 6, CNRS UMR 7614, 11 rue Pierre et Marie Curie, F-75231 Paris Cedex 05, France

E-mail: renata@cab.cnea.gov.ar

Received 19 April 2012, in final form 11 June 2012
Published 24 September 2012
Online at stacks.iop.org/JPhysB/45/194009

Abstract
We present a detailed study of the ionization probability of H_2O induced by a short intense laser pulse. Within the strong-field approximation, we present total and differential ionization probabilities of the water molecule fixed in space. It is shown that the second highest occupied molecular orbital (HOMO-1) dominates the single-electron emission process when the laser is polarized along the symmetry axis of the H_2O molecule, and that the electron emission is in general favoured in the direction along the laser polarization direction.

(Some figures may appear in colour only in the online journal)

1. Introduction

Since the pioneering experiments on ionization of fixed-in-space molecules by photon impact were performed almost two decades ago [1], there have been notable improvements in both photon sources and detection techniques. These experiments, where the molecule orientation may be resolved, are a fertile ground to study electron densities and molecular structures as well as reaction paths in controlled conditions, after interaction with photons [2–5].

Recently, ionization of oriented molecules by laser light has been proposed as an imaging method to determine electronic structures, nuclear geometries and chemical reactions [6, 7]. Proposed time-resolved imaging methods involve either the recording of ionization probabilities as a function of the angle between the photon polarization vector and the axis of the molecule or the use of two laser pulses in a pump-and-probe scheme [7, 8]. Very recently, the feasibility of some of these methods has been discussed in the framework of a theoretical time-dependent approach [9]. Experimentally, the orientation-dependent strong-field ionization yield was obtained for large polyatomic fixed-in-space molecules using state-of-the-art alignment and orientation techniques [7, 10].

Since experimental alignment of dipolar molecules, such as water, in field-free conditions is difficult to achieve a viable alternative method consists in working with non-aligned target molecules, measure the momenta of all fragments in coincidence after the interaction and reconstruct *a posteriori* the initial molecular orientation from the final-state data [11]. This is, however, a formidable task since four particles—one electron and up to three ions—must be recorded in coincidence after fragmentation of the H_2O molecule.

Despite these difficulties, ionization of water molecules receive intense attention because of its predominant role in applied areas. For instance, in medical physics, investigation of the direct effects of the radiation on water molecules, as well as the particle track that is created by the interactions, is a key part in radiotherapy investigations. In particular, ionization probabilities in a liquid phase are necessary to accurately describe the effects of radiation on living tissue, as required by simulations and dosimetry calculations. Recently, ionization cross-sections of liquid water by the impact of electrons were calculated in a perturbative theory [12].

A crucial issue in the development and implementation of ionization theories is the accurate description of complex molecular systems. Even relatively simple theories are hindered by the use of approximated wavefunctions for the unperturbed target that do not represent true molecular states. For instance, the use of a single-electron, single-centre pseudo-molecular description of the electronic orbitals of the molecules is customary.

[4] Author to whom any correspondence should be addressed.

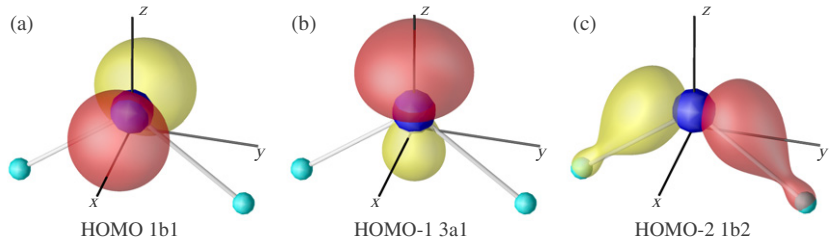

Figure 1. Isosurfaces of water orbitals: (a) HOMO, (b) HOMO-1 and (c) HOMO-2. The molecular reference frame is defined by the $\hat{x}$-, $\hat{y}$- and $\hat{z}$-axis. The oxygen and hydrogen position are $(0.22\hat{z})$ and $(\pm 1.42\hat{y} - 0.87\hat{z})$, respectively. The grey lines represent the distances between the O atom and each H.

Very recently, a method for water ionization cross-sections by fast proton impact within a first-order perturbative approximation was published [13]. The approach used a multiple-electron Slater determinant description of the target, expanded as a sum of Gaussian-type orbitals (GTOs). This versatile description has been worked out to obtain analytical expressions for the cross-sections, which may be easily included in dosimetry simulations. In the same spirit, we implement a method to investigate ionization of fixed-in-space H_2O molecules by interaction with short laser pulses in this work. The method involves the use of the strong-field approximation (SFA) [14–16] (see also [17]). The target is described in terms of a Slater determinant, where each orbital is expanded into a linear combination of GTOs. This choice of basis sets is motivated by the use of modern quantum-chemistry packages, which provide very accurate molecular ground states.

Simple first-order calculations, as the ones based on SFA, may not compete with state-of-the-art fully numerical methods based on the exact solution of the Schrödinger equation [18, 19]. On the other hand, fully *ab initio* methods are very difficult to extend to complex systems with more than one electron, and only recently the calculation of ionization of H_2 by intense ultrashort laser pulses [20] has been feasible. For H_2O, the problem must be drastically simplified even with today's computing power. Only very recently Petretti *et al* have been able to solve the four-dimensional time-dependent Schrödinger equation, after resorting to the single-active-electron approximation [9, 21].

However, the SFA is a simple, first-order theory with relatively low computational requirements, making it suitable for the evaluation of ionization probabilities of complex systems such as molecules or clusters. The goal of this work is therefore to describe and implement a SFA-type method that may be easily extended to large systems. We apply this method to analyse the ionization probability of water by short laser pulses, and its dependence on the orientation of the molecule relative to the polarization of the light. The contribution of each of the occupied orbitals is discussed in light of the results obtained in the present approximation. Atomic units are employed, except where otherwise stated.

2. Theory

We consider a fixed-in-space water molecule illuminated by a short laser pulse. The molecule is modelled as an N-electron system, whose evolution is governed by the time-dependent Hamiltonian

$$H(t) = H_0 + V_I(t), \tag{1}$$

where the interaction of the laser pulse with the N electrons in the length gauge is

$$V_I(t) = -\sum_{i=1}^{N} \boldsymbol{F}(t) \cdot \boldsymbol{r}_i.$$

The short six-cycle laser pulse considered in this work exerts a force on the system, proportional to its electric field:

$$\boldsymbol{F}(t) = F_0 \sin(\omega t)\, T(\omega t/2\pi)\, \hat{\varepsilon}, \tag{2}$$

where the trapezoidal envelope $T(x)$ is defined as

$$T(x) = \begin{cases} x/2 & \text{if} \quad 0 < x < 2 \\ 1 & \text{if} \quad 2 < x < 4 \\ (6-x)/2 & \text{if} \quad 4 < x < 6 \end{cases}$$

and vanishes in all other cases, ω is the central frequency, $\hat{\varepsilon}$ is the polarization vector and $\tau = 12\pi/\omega$ is the pulse duration.

The initial state $|\mathrm{i}\rangle$ is an eigenstate of the unperturbed, field-free, molecular system: $H_0|\mathrm{i}\rangle = E_0|\mathrm{i}\rangle$. The ionization amplitudes c_Ω at a time t are given, in the first-order perturbation theory by

$$c_\Omega(\boldsymbol{k}, t) = -\mathrm{i}\int_{t_0}^{t} \mathrm{d}t' \langle \boldsymbol{k}(t')|V_I(t')|\mathrm{i}\rangle\, \mathrm{e}^{-\mathrm{i}E_0 t}, \tag{3}$$

where the subscript Ω has been introduced to indicate that the target wavefunctions depend on the molecular spatial orientation.

Initially, the H_2O molecule is in the ground state, fixed in space and oriented as shown in figure 1. While the electron structure of multi-electron, nonlinear molecules, such as water, is difficult to describe theoretically in the present context, a usual approach is to simplify the multiple-centre molecular states by either one-centre wavefunctions, the solution of an effective central potential or linear combinations of atomic orbitals [22–24]. In this work, both the initial $|\mathrm{i}\rangle$ and final $|\boldsymbol{k}\rangle$ states are described by single-Slater determinants of spin-orbitals $\phi_1, \phi_2, \ldots, \phi_i, \ldots, \phi_N$ and $\phi_1, \phi_2, \ldots, \varphi_f, \ldots, \phi_N$, respectively [25]. The use of these states is based on the assumption that one electron has been promoted from a given orbital ϕ_i within the molecule to a continuum state φ_f with momentum $\boldsymbol{k}$, while the remaining electrons are kept frozen. The interaction V_I is expressed as a sum of one-electron interactions, and the amplitude reduces therefore to the matrix

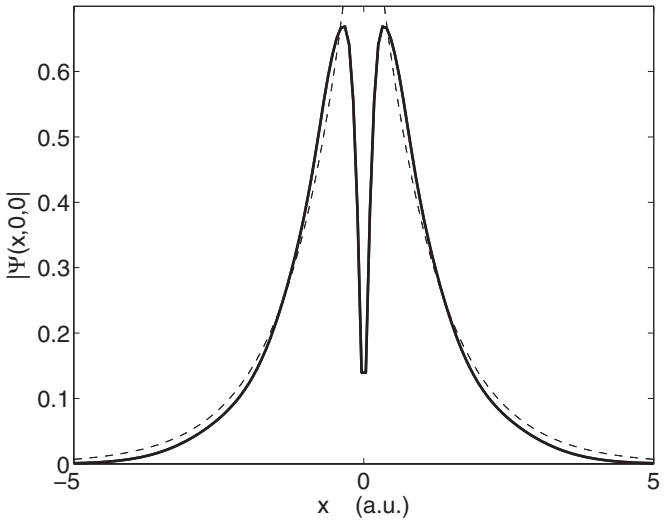

Figure 2. Probability density of the HOMO wavefunction along its symmetry axis x (full) is compared with the asymptotic expression (5) (dashed).

element between the two one-electron states involved in the transitions ϕ_i and φ_f.

The spatial part of bound orbitals is given as a linear combination of normalized GTOs, $G_{\alpha,j}$, centred on various nuclei α [13]:

$$\phi_i(\boldsymbol{r}) = \sum_{\alpha,j} c_{\alpha,j} G_{\alpha,j},$$
$$G_{\alpha,j}(\boldsymbol{r}_\alpha) = N_{\alpha,j}\, x_\alpha^{k_j}\, y_\alpha^{l_j}\, z_\alpha^{m_j}\, \exp(-\alpha_j r_\alpha^2), \tag{4}$$

where k_j, l_j and m_j are integers, $N_{\alpha,j}$ is the normalization constant of each GTO and the electronic coordinate relative to the nuclear centre α is denoted by $\boldsymbol{r}_\alpha$.

For a water molecule in the ground state, there are five orbitals occupied. The molecular orbitals used in this work have been obtained with the GAMESS(US) program [26] at the density functional level of theory with the Becke three-parameter hybrid exchange and the Lee–Yang–Parr gradient-corrected correlation B3LYP functional, cf [27] and [28] respectively. They have been obtained by geometry optimization and are the same as the ones used in [13]. The occupied orbital energies are shown in table 1, the highest occupied molecular orbital (HOMO) having an energy of $E_i = -0.49$ au. In figure 1, we show the reference frame used, as well as the isosurfaces, for the electronic density of the three higher occupied orbitals when $|\phi_i(\boldsymbol{r})|^2 = 0.1$.

The GTO basis employed, with 36 functions, produce results that at large distances, and in the region of the largest contribution to the matrix elements, agree within a few per cent with the asymptotic expansion

$$r^{Z/\kappa-1}\, \exp(-\kappa r), \tag{5}$$

where κ is the momentum associated with the ionization potential $I_P = \kappa^2/2$. This agreement is shown in figure 2, where the GTO-expanded wavefunction and the asymptotic expresion for the HOMO in the direction of its maximum (x-axis) are displayed. Similar agreement is obtained for the other orbitals.

Table 1. Occupied orbitals of the water molecules with the corresponding ionization energies E_i, calculated at the equilibrium position.

Orbital	Symmetry	E_i (au)
HOMO	1_{b1}	−0.49
HOMO-1	3_{a1}	−0.57
HOMO-2	1_{b2}	−0.71
HOMO-3	2_{a1}	−1.35
HOMO-4	1_{a1}	−20.55

In the SFA, the final state for the emitted electron is written as a Volkov wave, thereby neglecting its interaction with the remaining ionic molecule, and describing it as a free electron evolving in the field of the laser:

$$\varphi_f(\boldsymbol{r}, t) = \left(\frac{1}{2\pi}\right)^{3/2} \exp\{\mathrm{i}[\boldsymbol{k} + \boldsymbol{A}(t)] \cdot \boldsymbol{r} - \mathrm{i}S(k,t)\}. \tag{6}$$

Here, the Volkov phase is

$$S(k,t) = \frac{1}{2}\int_0^t \mathrm{d}t'\, [\boldsymbol{k} + \boldsymbol{A}(t')]^2, \tag{7}$$

and $\boldsymbol{A}(t) = -\int_0^t \mathrm{d}t' \boldsymbol{F}(t')$ is the vector potential of the electric field.

Finally, taking into account the spin degeneracy, the differential ionization probability for the emission of an electron with energy $E = k^2/2$ into the solid angle element $\mathrm{d}\Omega_k$ at the end of the pulse is given by [17]

$$\frac{\mathrm{d}P}{\mathrm{d}E\mathrm{d}\Omega_k} = 2k\,|c_\Omega(\boldsymbol{k}, \tau)|^2, \tag{8}$$

where

$$c_\Omega(\boldsymbol{k}, \tau) = -\mathrm{i}(2\pi)^{-3/2} \int_0^\tau \mathrm{d}t\; \boldsymbol{F}(t) \cdot \langle \mathrm{e}^{\mathrm{i}(\boldsymbol{k}+\boldsymbol{A})\cdot\boldsymbol{r}} |\, \boldsymbol{r}\, | \phi_i \rangle\, \mathrm{e}^{\mathrm{i}(S - E_i t)} \tag{9}$$

and the time integration was performed by a low-order rectangular quadrature method, where convergence was checked by systematically decreasing the time step. Also, in some cases, a variable-step Simpson quadrature calculation was independently performed to test the accuracy of the results.

Several approximations were performed in order to arrive to the above expression (9). The main shortcomings are the non-orthogonality of the initial and final states for the active electron, and the well-known disagreements between the length and velocity gauges in the SFA [29, 30]. There is no unanimous opinion on which gauge is the most convenient for each problem. While Awasthi *et al* found that for H_2 the Coulomb-corrected velocity gauge produces better total probability ionization results [31]; the dependence on orientation has been found to be better described by the length gauge [32]. Also, the velocity gauge has been shown to be more sensitive to the parity of the initial state wavefunction [33, 34]. We therefore believe that the main physics is captured by the present approach and postpone studies based on fewer approximations for future work.

Since we expand the initial orbitals into GTOs, the space integrals can be solved analytically:

$$\langle \mathrm{e}^{\mathrm{i}\boldsymbol{q}\cdot\boldsymbol{r}} |\, \boldsymbol{r}\, | \phi_i \rangle = \sum_{\alpha,j} c_{\alpha,j} N_{\alpha,j}\, \exp(-\mathrm{i}\boldsymbol{q}\cdot\boldsymbol{R}_\alpha)\, \exp(-q^2/4\alpha_j)$$
$$\times\, (\pi/\alpha_j)^{3/2}\, (2\mathrm{i}\sqrt{\alpha_j})^{-(k_j+l_j+m_j)}$$
$$\times\, \{\boldsymbol{R}_\alpha\, H_{k_j}(q_{xj})\, H_{l_j}(q_{yj})\, H_{m_j}(q_{zj}) + \boldsymbol{I}_j\},$$

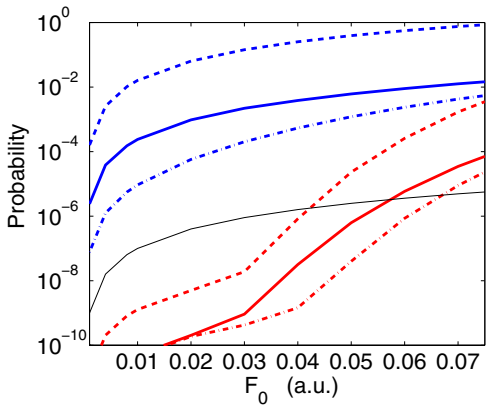

Figure 3. Total ionization probability from HOMO orbitals (solid line), HOMO-1 (dashed line), and HOMO-2 (dash–dotted line) of water, when the polarization vector points in the $\hat{z}$ direction, and frequencies of the pulse are $\omega = 0.6$ au (larger probabilities, in blue) and $\omega = 0.057$ au (red). The thin black solid line shows the form of the function F_0^2, which dominates the qualitative shape of the ionization probability for the highest frequency.

where $\boldsymbol{R}_\alpha = (X_\alpha, Y_\alpha, Z_\alpha)$ is the position of each nuclei of H_2O, and the vector $\boldsymbol{I}_j$ is defined as

$$\boldsymbol{I}_j = \frac{1}{2\mathrm{i}\sqrt{\alpha_j}} \begin{pmatrix} H_{k_j+1}(q_{xj})\, H_{l_j}(q_{yj})\, H_{m_j}(q_{zj}) \\ H_{k_j}(q_{xj})\, H_{l_j+1}(q_{yj})\, H_{m_j}(q_{zj}) \\ H_{k_j}(q_{xj})\, H_{l_j}(q_{yj})\, H_{m_j+1}(q_{zj}) \end{pmatrix}, \qquad (10)$$

where $q_{ij} = q_i/(2\sqrt{\alpha_j})$, q_x, q_y and q_z are the components of the vector $\boldsymbol{q} = \boldsymbol{k} + \boldsymbol{A}$ in the molecular frame, as defined in figure 1, and $H_n(x)$ are the Hermite polynomials of order n. The reduction of these kinds of integrals to simple analytical expressions when using GTOs has proved very valuable for fast numerical evaluation of molecular transitions by interactions with particles [13] and photons. In the latter case, the use of simple approximations in combination with description of the target using linear combinations of GTOs have provided valuable information on laser-ionization of relatively large molecules (see for instance [32] and references therein).

3. Spectra for H_2O

We investigate ionization probabilities of the water molecule by interaction with short laser pulses within the SFA theory described in the previous section. Calculations were performed in different regions of the spectrum, allowing us to probe the tunnelling and multiphotonic ionization regimes. We consider two six-cycle pulses: one in the ultra-violet, with frequency $\omega = 0.6$, and the other in the near-infrared, $\omega = 0.057$ au ($\lambda = 800$ nm), with duration pulses $\tau = 1.5$ and 16 fs, respectively.

In figure 3, we show total ionization probability equation (8), integrated in electronic emission angles Ω_k and energy E, as a function of the amplitude of the laser field F_0. The integration in the electron momenta angles was performed by averaging 100–200 random electron-emission directions. The molecular reference frame is defined such that the oxygen atom is located on the $\hat{z}$-axis and the two H atoms are in the yz plane, symmetrically located with respect to the $\hat{z}$-axis. Thus, the molecule is in the plane yz, as shown in figure 1. The laser light is polarized along the z direction, with frequencies $\omega = 0.6$ (in blue) and 0.057 au (in red).

The probabilities for ionization from different orbitals are displayed separately. As can be observed in the figure, the probabilities for the highest frequency are several orders of magnitude larger than for 800 nm. It is also shown that the ionization from the HOMO-1 is significantly more probable than from the other orbitals.

The Keldysh parameter $\gamma = \sqrt{I_p/2U_p}$ (where I_p is the ionization potential and $U_p = F_0^2/4\omega^2$ is the ponderomotive energy) separates two qualitatively distinct neighbouring domains [17]: $\gamma < 1$ defines the tunnelling regime, while $\gamma > 1$ defines the multiphotonic domain. The laser pulse with frequency $\omega = 0.6$ au belongs to the last case for all the intensity-range investigated here. The basic scaling law for the multiphoton-ionization rate for the absorption of n photons is proportional to the nth power of the laser photon flux $I(\omega)/\hbar\omega$ (see for instance review [35]). For relatively low-intensity lasers, the ionization probability is then dominated by absorption of a small number of photons. This scaling law is consistent with the shape of the curves for $\omega = 0.6$ au in figure 3, that are proportional to the laser intensity $I = F_0^2$, indicating that, in the complete range of intensities investigated, the total ionization probabilities are dominated by the absorption of one photon. However, one should remark that for this frequency and the HOMO-2, a second-order theory may significantly increase the ionization yield since possible resonances—not described in SFA—may be observed, cf for example [36]. This one-photon-ionization behaviour breaks down for 800 nm laser pulses, where the energy of a single photon with the central frequency is not enough to ionize the water molecule.

More detailed information may be obtained by analysing the energy-differential electron-emission ionization probabilities. In figure 4, we show water ionization probabilities as a function of the electron energy, integrated over the emission angles Ω_k, for fixed orientation of the molecule. The laser pulses are polarized in the z direction, with amplitude $F_0 = 0.07$ au, and frequencies $\omega = 0.057$ (upper panel) and $\omega = 0.6$ au (lower panel). ATI peaks appear at energies $E_n = E_i + n\omega - U_P$, where n is the number of absorbed photons. The arrows in the lower panel indicate roughly the final electron energy regions following absorption of one, two or three photons with the initial state being HOMO, HOMO-1 or HOMO-2. As already observed in the total ionization probabilities (figure 3), the ionization from orbital HOMO-1 is considerably larger than the other orbitals at both frequencies investigated. The ionization probabilities from HOMO-3 and HOMO-4 (not shown) are much smaller.

Spectra in figure 4 also show that for ionization from HOMO-2, the first ATI peak is suppressed at the highest frequency. This suppression of the lowest energy peak was first observed almost three decades ago [37] and has been theoretically confirmed and interpreted within the framework of perturbation theory [38, 39], and within an analysis of the ponderomotive forces and the dynamical shifting of the ionization threshold due to the ponderomotive potential [40] (see also pages 252–3 of [35]).

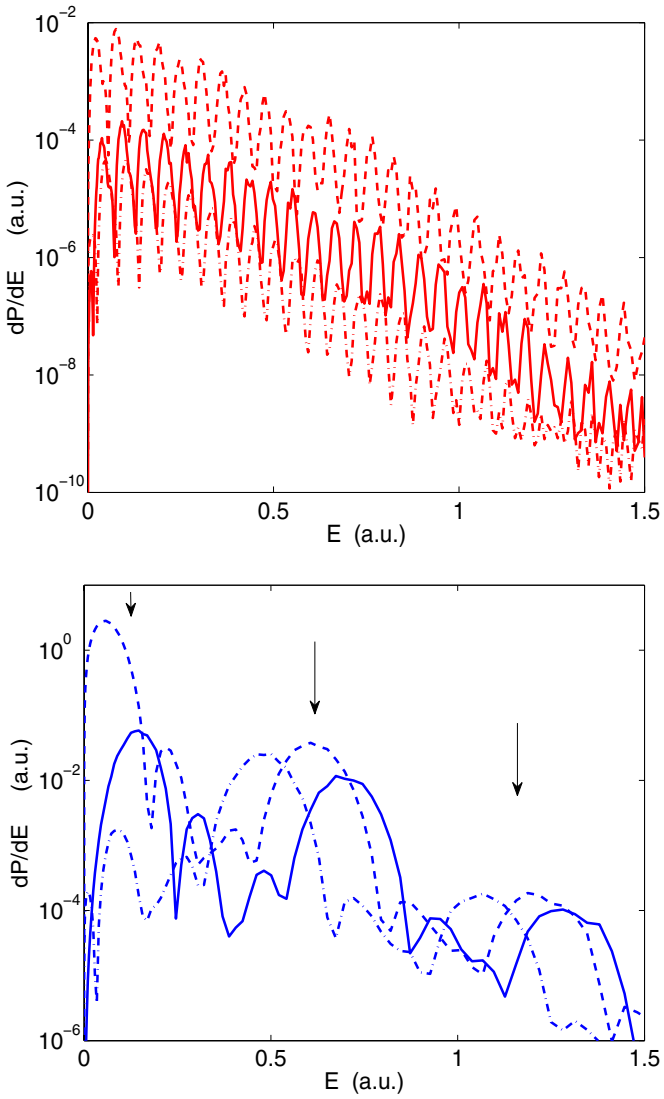

Figure 4. Differential ionization probability integrated in emission angles. $F_0 = 0.07$ au, $\hat{\varepsilon} \parallel z$, $\omega = 0.057$ (upper pannel) and 0.6 au (lower pannel). (Full line) emission from HOMO; (dashed line) from HOMO-1; (dash–dotted line) HOMO-2. The arrows indicate the approximate energy of the peaks E_n for absorption of one, two and three photons (see the text).

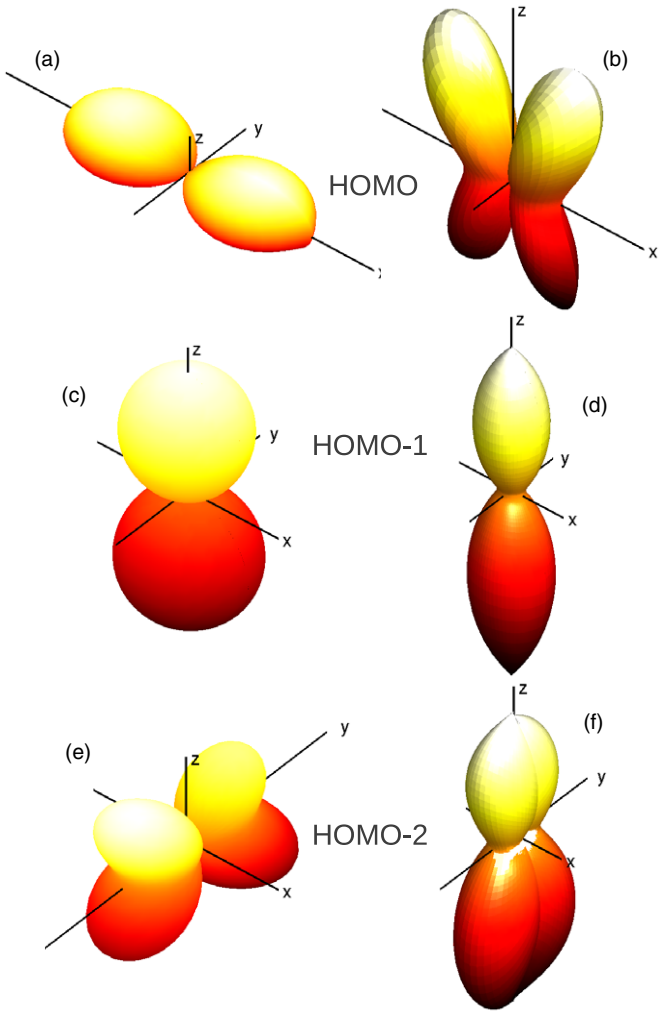

Figure 5. Angle-differential ionization probabilities (integrated in energy) of H_2O by laser pulses of frequencies $\omega = 0.6$ au (left column) and $\omega = 0.057$ au (right column). The laser amplitude is $F_0 = 0.07$ au and the polarization is in the z direction. The contribution of each orbital to the ionization probability is plotted in arbitrary units: (a) and (b) ionization from HOMO orbital, (c) and (d) from HOMO-1 and (e) and (f) from HOMO-2. The maximum extension of the z-axis for each figure is (a) 0.083, (b) 1.7×10^{-6}, (c) 0.22, (d) 1.1×10^{-4}, (e) 0.5×10^{-4}, and (f) 3.0×10^{-8}.

In order to analyse the contributions to the observed ionization-rate spectra arising from each occupied orbital, in figure 5 we present angular emission probabilities. They were obtained by integration of equation (8) on electron energies. The laser pulses have polarization along the z-axis, with amplitude $F_0 = 0.07$ au and frequencies $\omega = 0.6$ au, for the data in the left column, (figure 5 (a), (c) and (e)) and $\omega = 0.057$ au in the right column (figure 5 (b), (d) and (f)). The plots are in arbitrary units to compare the shape of the distributions, but the absolute intensity may be deduced easily, since integration over emission angles gives the total ionization probabilities of figure 3.

We observe that the electron emission from HOMO lies preferentially on the plane zx, perpendicular to the molecular plane zy; ionization from HOMO-1 has two lobes aligned with the z-axis, following the polarization vector, and the emission from HOMO-2 is mainly produced on the molecular plane. These features are consistent with the shape of the orbitals (see figure 1). The electronic density of HOMO form two lobes in the x direction, giving a higher probability of emission in that direction and in the plane perpendicular to the molecular plane. The HOMO-1 have two deformed lobes along the z direction, being the most easily ionized orbital when the polarization points in the z direction. Finally, the HOMO-2 have two deformed lobes around the two directions OH, making the emission probabilities most significant in the molecular plane.

The ionization spectra are obtained from the added contributions of all occupied orbitals. Figure 6 shows the emission probability $dP/d\Omega_k$, summed from all orbitals of the H_2O molecule. We consider the two six-cycle laser pulses as before, with $\omega = 0.6$ and 0.057 au and intensity $F_0 = 0.07$ au. In figures 6(a) and (b) the polarization is in the z direction.

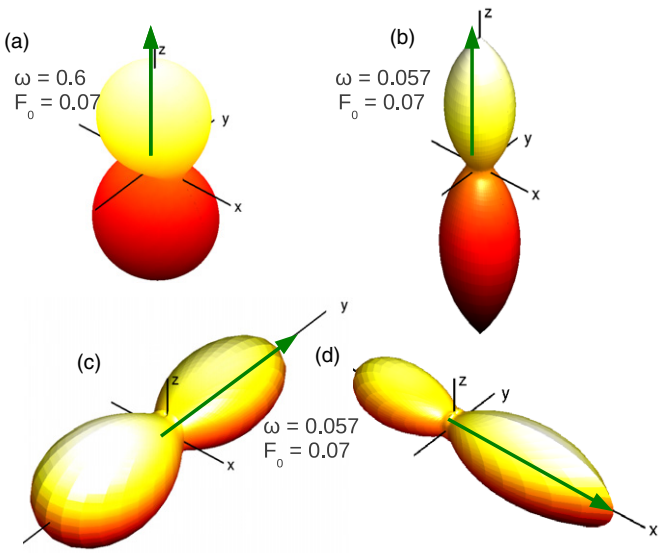

Figure 6. Angular distributions of ionization probabilities integrated in energy, with the contribution of all orbitals. The plots are given in arbitrary units to show the qualitative behaviour of the data. The water molecule is fixed as shown in figure 1 and the (green) arrow indicates the laser polarization. The laser amplitude is $F_0 = 0.07$ and the frequencies are: (a) $\omega = 0.6$ au, and (b), (c) and (d) $\omega = 0.057$ au. The maximum extension of the z axis for each figure is (a) 0.23, (b) 1.1×10^{-4}, (c) 9.6×10^{-6} and (d) 4.8×10^{-5}.

As we discussed before, the contribution of ionization from HOMO-1 is considerably more important than from the other orbitals. Then, the overall spectra basically resembles the angular distributions of electrons ionized from this orbital (compare figures 6(a) and (b) with figures 5(c) and (d)).

In order to analyze the effects of molecule orientation relative to the laser polarization, in figures 6(c) and (d) we also consider polarization along the y- and x-axis, respectively. These plots indicate clearly that there is a preferential emission in the direction of the laser polarization.

However, we do not know what orbitals give the principal contribution for these polarization directions. In order to elucidate this, in figure 7 we show the contributions of ionization from each orbital as a function of the orientation of the polarization vector. In this figure, we present total ionization probabilities P as a function of the polar angle θ and azimuthal angle ϕ of the polarization vector $\hat{\varepsilon}$ with respect to the molecular reference frame. The sum of each of the contributions (b), (c) and (d) is shown in (a).

We observe that the total probability is maximal when the polarization is directed along the $\pm z$ direction ($\theta = 0$ or π), or when it lies in the plane xz ($\phi = 0$ or π). In each case, the major contribution comes from HOMO-1 or HOMO, respectively. A minimum in the ionization probability occurs when the polarization is on the $\pm y$ direction ($\theta = \pi/2$ and $\phi = \pi/2$ or $3\pi/2$), perpendicular to the molecular plane.

In the previous analysis, we have concluded that ionization from the HOMO-1 gives the largest contribution when the polarization is on the z axis. This phenomenon can be clearly observed in figure 7 for $\theta = 0$. Now, we can also say that if the polarization is in the $\pm x$ direction ($\theta = \pi/2$ and $\phi = 0$, or π), the principal contribution comes from the HOMO. These conclusions are in agreement with the recent work of Petretti *et al* [9], obtained by the solution of the time-dependent Schrödinger equation for lower intensity pulses of 800 nm lasers. For other orientations of $\hat{\varepsilon}$, we observe a combination

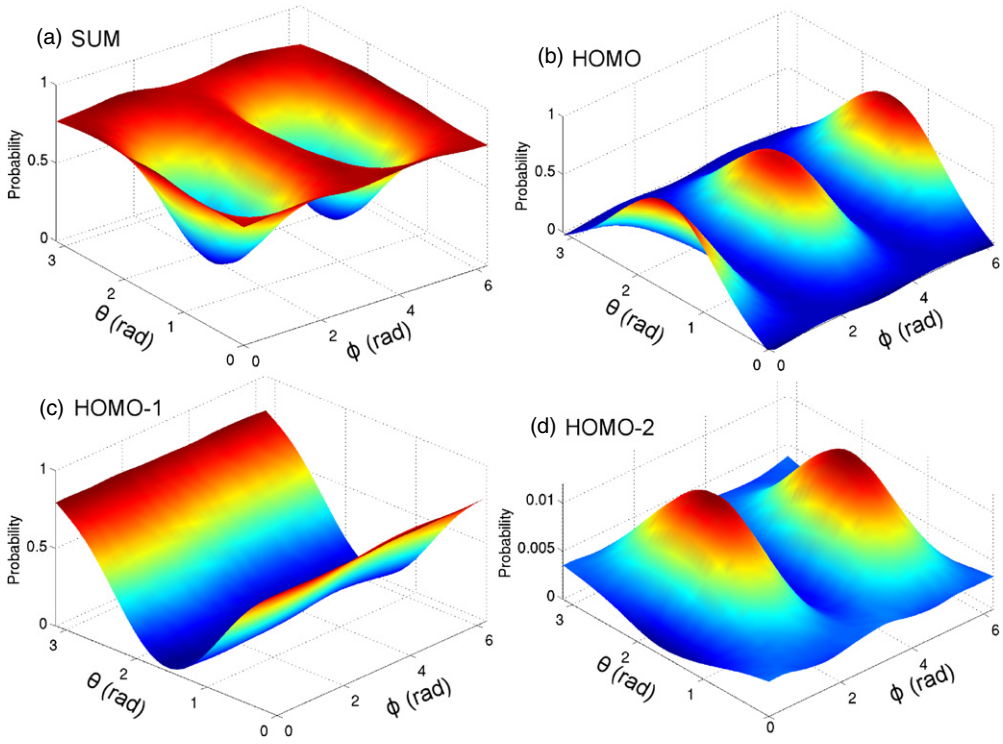

Figure 7. Water total ionization probabilities as a function of the polarization direction: (a) sum of contributions of all orbitals, (b) ionization from HOMO, (c) from HOMO-1 and (d) from HOMO-2. The laser amplitude is $F_0 = 0.07$ au and the frequency is $\omega = 0.6$ au.

of contributions from both orbitals. Ionization from HOMO-2 and more strongly bound orbitals are, in all cases, very small compared to these two higher orbitals.

4. Conclusions

We have employed the strong-field approximation to study multiphoton ionization of H_2O molecules by linear-polarized short intense laser pulses with two frequencies ($\omega = 0.057$ and 0.6 au). We take into account all the electrons in the target and represent the initial and final states by Slater determinants. The bound state wavefunctions are proposed as linear combinations of Gaussian-type orbitals while the continuum state of the emitted electron is represented by a Volkov wavefunction, which includes to all orders the interaction between the electron and the laser field.

From the transition amplitude, we obtain differential probabilities as a function of the electron emission angle and energy, and the total probability for electron emission from the different occupied molecular orbitals. We observe that for the highest frequency, the total probability is linear with the field intensity, while for low frequencies this behaviour breaks down. In all the cases we have studied, it is seen that electron emission probability is largest from the HOMO-1 initial state. The electron energy distributions show the ATI peaks, and the results for different initial orbitals are shifted due to different binding energies. The angular distributions show characteristic shapes which more or less mimic the form of the initial state orbital, while the total emission probability as a function of emission angle shows a typical dipolar distribution in the direction of the electric field.

On the other hand, some general conclusions, as the similarity of the molecular orbital shape and of the angular distributions, and principal contributions from HOMO or HOMO-1 depending on the laser polarization, have also been recently obtained in the complex framework of a theoretical time-dependent approach [9]. These results show the power of the present simple method to investigate ionization of molecules by interaction with short laser pulses with comparatively computational low cost.

Acknowledgments

This work was partially supported by the Consejo Nacional de Investigaciones Científicas y Técnicas (grant PIP 112-2009-0100166), Universidad Nacional de Cuyo (grant 06/C340), Argentina and from the EU Seventh Framework Programme under grant agreement PIRSES-GA-2010-269243.

References

[1] Shigemasa E, Adachi J, Oura M and Yagishita A 1995 *Phys. Rev. Lett.* **74** 359–62
[2] Adachi J, Motoki S, Cherepkov N A and Yagishita A 2002 *J. Phys. B: At. Mol. Opt. Phys.* **35** 5023–33
[3] Motoki S, Adachi J, Ito K, Ishii K, Soejima K, Yagishita A, Semenov S K and Cherepkov N A 2002 *J. Phys. B: At. Mol. Opt. Phys.* **35** 3801–19
[4] Landers A *et al* 2001 *Phys. Rev. Lett.* **87** 013002
[5] Osipov T, Cocke C L, Prior M H, Landers A, Weber Th, Jagutzki O, Schmidt L, Schmidt-Böcking H and Dörner R 2003 *Phys. Rev. Lett* **90** 233002
[6] Lin C D, Le A-T, Chen Z, Morishita T and Lucchese R 2010 *J. Phys. B: At. Mol. Opt. Phys.* **43** 122001
[7] Hansen J L, Holmegaard L, Nielsen J H, Stapelfeldt H, Dimitrovski D and Madsen L B 2012 *J. Phys. B: At. Mol. Opt. Phys.* **45** 015101
[8] Hansen J L *et al* 2011 *Phys. Rev.* A **83** 23406
[9] Petretti S, Saenz A, Castro A and Decleva P 2012 *Chem. Phys.* (doi:10.1016/j.chemphys.2012.01.011)
[10] Hansen J L, Stapelfeldt H, Dimitrovski D, Abu-Samha M, Martiny C P J and Madsen L B 2011 *Phys. Rev. Lett* **106** 073001
[11] Yamazaki M, Adachi J, Teramoto T, Yagishita A, Stener M and Decleva P 2009 *J. Phys. B: At. Mol. Opt. Phys.* **42** 1001
[12] de Sanctis M L, Politis M-F, Vuilleumier R, Stia C R and Fojón O A 2012 *J. Phys. B: At. Mol. Opt. Phys.* **45** 5206
[13] Dubois A, Carniato S, Fainstein P D and Hansen J P 2011 *Phys. Rev.* A **84** 012708
[14] Keldysh L V 1964 *Zh. Eksp. Teor. Fiz.* **47** 1945–57
Keldysh L V 1964 *Sov. Phys.—JETP* **20** 1307 (Engl. Transl.)
[15] Faisal F H M 1973 *J. Phys. B: At. Mol. Opt. Phys.* **6** L89–92
[16] Reiss H R 1980 *Phys. Rev.* A **22** 1786–813
[17] Milosevic D B, Paulus G G, Bauer D and Becker W 2006 *J. Phys. B: At. Mol. Opt. Phys.* **39** R203–62
[18] Bauer D and Koval P 2006 *Comput. Phys. Commun.* **174** 396–421
[19] Yuan K-J, Lu H and Bandrauk A D 2011 *Phys. Rev.* A **83** 043418
[20] Vanne Y V and Saenz A 2010 *Phys. Rev.* A **82** 011403
[21] Petretti S, Vanne Y V, Saenz A, Castro A and Decleva P 2010 *Phys. Rev. Lett.* **104** 223001
[22] Errea L F, Illescas C, Méndez L, Pons B, Rabadán I and Riera A 2007 *Phys. Rev.* A **76** 040701
[23] Champion C, Boudrioua O and Cappello C D 2008 *J. Phys. Conf. Ser.* **101** 012010
[24] Champion C and Rivarola R D 2010 *Phys. Rev.* A **82** 042704
[25] Bransden B H and Joachain C J 1983 *Physics of Atoms and Molecules* (Harlow: Longman Scientific & Technical)
[26] Schmidt M W *et al* 1993 *J. Comput. Chem.* **14** 1347–63
[27] Becke A D 1993 *J. Chem. Phys.* **98** 1372–7
[28] Lee C, Yang W and Parr R G 1988 *Phys. Rev.* B **37** 785–9
[29] Schlicher R R, Becker W, Bergou J and Scully M O 1984 *Quantum Electrodynamics and Quantum Optics (NATO Advanced Study Institute Series B* vol 10*)* ed O Barut (New York: Plenum) p 405
[30] Burlon R, Leone C, Trombetta F and Ferrante G 1987 *Il Nuovo Cimento* D **9** 1033–54
[31] Awasthi M, Vanne Y V, Saenz A, Castro A and Decleva P 2008 *Phys. Rev.* A **77** 63403
[32] Kjeldsen T K, Bisgaard C Z, Madsen L B and Stapelfeldt H 2005 *Phys. Rev.* A **71** 13418
[33] Bauer D, Milošević D B and Becker W 2005 *Phys. Rev.* A **72** 023415
[34] Chen Y J and Hu B 2009 *Phys. Rev.* A **80** 033408
[35] Eberly J H, Javanainen J and RzZewski K 1991 *Phys. Rep.* **204** 331–83
[36] Guichard R, Bachau H, Cormier E, Gayet R and Rodríguez V D 2007 *Phys. Scr.* T **76** 397–409
[37] Kruit P, Kimman J, Muller H G and van der Wiel M J 1983 *Phys. Rev.* A **28** 248–55
[38] Gontier Y and Trahin M 1980 *J. Phys. B: At. Mol. Opt. Phys.* **13** 4383–90
[39] Bucksbaum P H, Bashkansky M, Freeman R R, McIlrath T J and Dimauro L F 1986 *Phys. Rev. Lett.* **56** 2590–3
[40] Muller H G and Tip A 1984 *Phys. Rev.* A **30** 3039–50